TURBULENCE SIMULATIONS OF X-POINT PHYSICS ON THE L-H TRANSITIONS[1]

X. Q. XU,[1], R. H. COHEN[1], W. M. NEVINS[1], G. D. PORTER[1], M. E. RENSINK[1], T. D. ROGNLIEN[1], J. R. MYRA[2], D. A. D'IPPOLITO[2], R. MOYER[3], P. B. SNYDER[4], T. N. CARLSTROM[4]

[1)] Lawrence Livermore National Laboratory Livermore, CA 94551, USA
[2)] Lodestar Research Corporation, Boulder, CO 80301 USA
[3)] University of California, San Diego, La Jolla, CA 92093 USA
[4)] General Atomics, San Diego, CA 92186 USA

e-mail contact of main author: xxu@llnl.gov

Abstract. The resistive X-point mode is shown to be the dominant mode in boundary plasmas in X-point divertor geometry. The poloidal fluctuation phase velocity from the simulation results of the resistive X-point turbulence shows experimentally measured structure across separatrix in many fusion devices. The fluctuation phase velocity is larger than $E \times B$ velocity both in L and H mode phases. It is also demonstrated that there is a strong poloidal asymmetry of particle flux in the proximity of the separatrix. Turbulence suppression in the L-H transition results when sources of energy and particles drive sufficient gradients as in the experiments.

1. INTRODUCTION

The performance of tokamaks and other toroidal magnetic devices depends crucially on the dynamics of the boundary region, i.e., the transition region from the hot core plasma through the separatrix to the material surface of the first wall. Plasma turbulence, and the resulting anomalous cross-field plasma transport, are crucial physics processes in the boundary region, affecting both core plasma confinement and plasma-wall interactions. Reduction of anomalous plasma transport at the boundary, associated with the transition to the H-mode operating regime, leads to sharp pedestal-like structures in the temperature and density profiles. The ubiquity of the L-H transition indicates some robust, 'universal' ingredient, such as $\boldsymbol{E} \times \boldsymbol{B}$ shear suppression which has been invoked for both internal and the H-mode transport barriers [1]. The fact that changes seem to be precipitated at the outer midplane is suggestive of mechanisms based on the stabilization of the ballooning modes or suppression of turbulent transport by radial electric field shear [2].

Although the H-mode can be realized in a wide variety of toroidal systems, it is most clearly associated with divertor tokamaks possessing a separatrix. It has been observed in DIII-D [3] and JET [4] that the number of X-points and their locations in divertor configurations play an important role in determination of the H-mode power threshold. This threshold is usually higher in double-null (DN) divertors than in single-null (SN) divertors and is lower for the case of the ion ∇B drift towards the X-point than the ion ∇B drift away from the X-point in SN divertors. It has been argued that the power threshold is not

[1]Work performed under the auspices of the U. S. Department of Energy by University of California Lawrence Livermore National Laboratory under contract W-7405-ENG-48, DE-FG03-97ER54392 at LRC, and DE-FG03-95ER54294 at UCSD.

due to intrinsic midplane plasma parameters alone, but rather parameters at the plasma edge or in the scrape-off-layer (SOL) plasma which depend on the field line geometry [5]. Our previous work provides physical understanding using BOUT (a 3D nonlocal electromagnetic turbulence code) simulations [6]. BOUT models boundary-plasma turbulence in a realistic divertor geometry using Braginskii equations [7] for plasma vorticity, density (n_i), electron and ion temperature (T_i, T_e) and parallel momentum. It has been found that X-point damping coupled with the change in boundary plasma flow direction plays a crucial role in determination of the fluctuation levels. The BOUT simulation results predict smaller fluctuation levels in the case of the ion ∇B drift towards the X-point than the ion ∇B drift away from the X-point in SN divertor tokamaks due to a change in boundary plasma flow direction away from the X-point that impacts the strong damping near the divertor X-point [8]. The sensitivity is less in systems possessing up-down symmetry, such as a tokamak with a circular cross-section and symmetric DN divertor configurations. Theoretical symmetry considerations lead to a similar conclusion [9].

In addition to the complexity of the nonlinear dynamics of the turbulence (and unlike core plasmas), the fluctuation levels in edge plasmas are comparable to mean values and the time and spatial scales of turbulence can be comparable to that of the background parameters. To simulate a dynamically steady state in the plasma boundary would require coupling the turbulence to the evolution of averaged profiles, including realistic particle and energy sources and sinks. That requires carrying out the calculation over a transport time scale, typically on the order of $\sim 50ms$. Such a long calculation is difficult if not impossible with present computer capabilities for large-scale turbulence calculations like BOUT. However, the L-H transition typically takes place on a turbulent nonlinear time scale $< 100\mu s$ [2] and BOUT is able to capture the transition dynamics.

The remainder of the paper is organized as follows. Section II discusses X-point effects on boundary turbulence and its characteristics. Results concerning the dynamics of the L-H transition are given in Sec. III. Finally, a summary of this paper is presented in Sec. IV.

2. Boundary turbulence with X-point geometry

Early stability and turbulence studies indicated that the separatrix geometry together with characteristically steep gradients at the edge of H-mode discharges tends to introduce strong stabilizing effects for MHD ballooning modes when the X-point region has good curvature [10] and greatly reduce the turbulent thermal conductivity due to electrostatic resistive ballooning modes [11]. The classical resistive ballooning modes fall into two separated classes based on the ordering of the resistive time scale [12]: (i) those driven by $\Delta_B^{'}$ (the stability index for resistive ballooning), the energy source from ideal region and (ii), Carreras-Diamond-type modes, driven by pressure gradients in the non-ideal region. The class (i) mode is unstable only if very close to the ideal MHD stability ballooning boundary, $\beta \sim \beta_{ideal}$, where $\Delta_B^{'} \rightarrow \infty$. The necessary condition for the class (ii) mode is that its growth rate, γ, must exceed the sound frequency, i.e., that $\gamma > c_s/qR$, with c_s being the sound speed, R the major radius, and q the safety factor. Since for circular geometry this constraint can be expressed as a condition on the toroidal mode number n, $n > const./q^{5/2}$, it suggests that the mode is always unstable in the H-mode pedestal of a separatrix plasma boundary where $q \rightarrow \infty$. The RX mode discussed here is the physical manifestation of the class (ii) modes in X-point geometry.

2.1 Resistive X-point modes

Recent studies of the resistive ballooning modes in the boundary plasma of diverted tokamaks have been performed within the framework of a collisional fluid model [8, 13, 14]. It is shown that the large magnetic shear and small poloidal field in the X-point region act to increase the wavenumber, and hence the importance of the resistivity, near the X-point. The resulting "disconnection" of the eigenmodes across the X-point profoundly influences the unstable spectrum. A new class of modes called resistive X-point (RX) modes exploits this synergism between resistivity and the X-point geometry, giving rise to robust growth rates at moderate-to-low mode numbers. Relative to an equivalent limited plasma, the diverted plasma is shown to be more unstable in the edge (inside the separatrix), and more stable in the scrape-off-layer. The radial profiles of linear mode characteristics in L-mode calculated from the linear stability code BAL [14] are given in Figures (1). Since

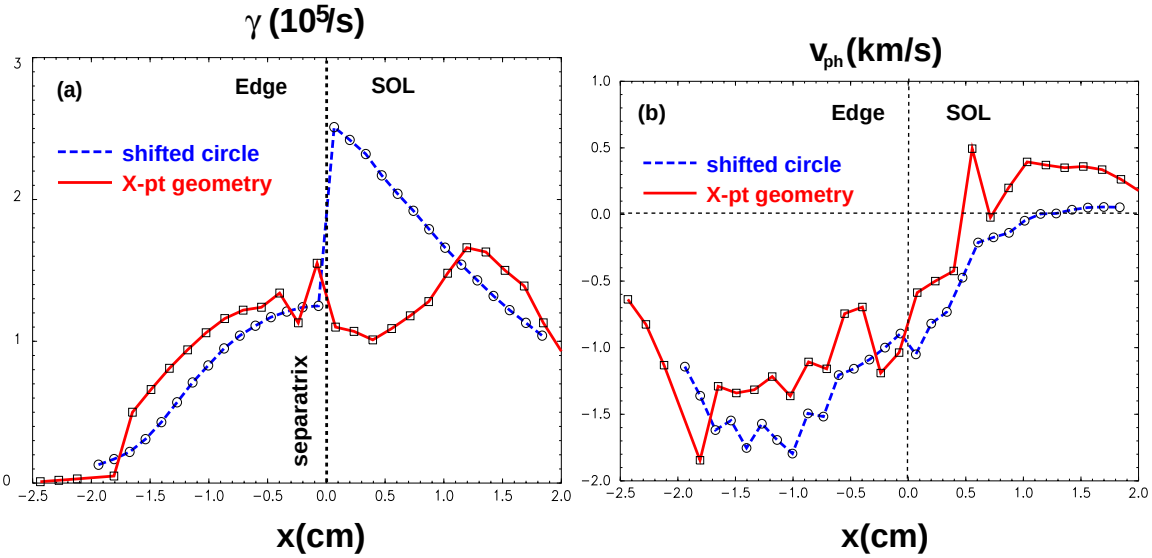

FIG. 1: (a) Linear growth rate of the RX mode in X-point and shifted circle geometries; and (b) The poloidal phase velocity in the $\boldsymbol{E} \times \boldsymbol{B}$ drift frame of RX mode in X-point and shifted circle geometries from linear calculation

the mode number for the most unstable mode in the X-point geometry is roughly constant ($n \sim$ 40-80) in the proximity of the separatrix ($x \sim \pm 1.5cm$), the profile of the phase velocity is similar to the profile of the real frequency ($\omega = k_p v_{ph}$ and $k_p = nB/RB_p$). The RX mode is analogous to class (ii) modes in the X-point geometry. However, the simple analytical solution of the class (ii) mode is not applicable in the boundary region across the separatrix because the two scale analysis is not valid for X-point geometry due to the very strong poloidal magnetic shear structure.

Most properties of RX turbulence in boundary plasmas are consistent with the various fluctuation measurements. From the correlation function, parameters like correlation time, poloidal correlation length and poloidal propagation velocity have been extracted from the BOUT simulations to characterize the fluctuations on DIII-D. The poloidal phase velocity v_{ph} of the potential fluctuations in the midplane (Figures 2(a)) is in the ion drift direction and becomes negative (electron drift direction) close to the last closed flux surface (LCFS) and into the edge of the main plasma. The phase velocity is obtained from a least-squares fit of a line to the curve of constant phase which passes through the origin of the two-point

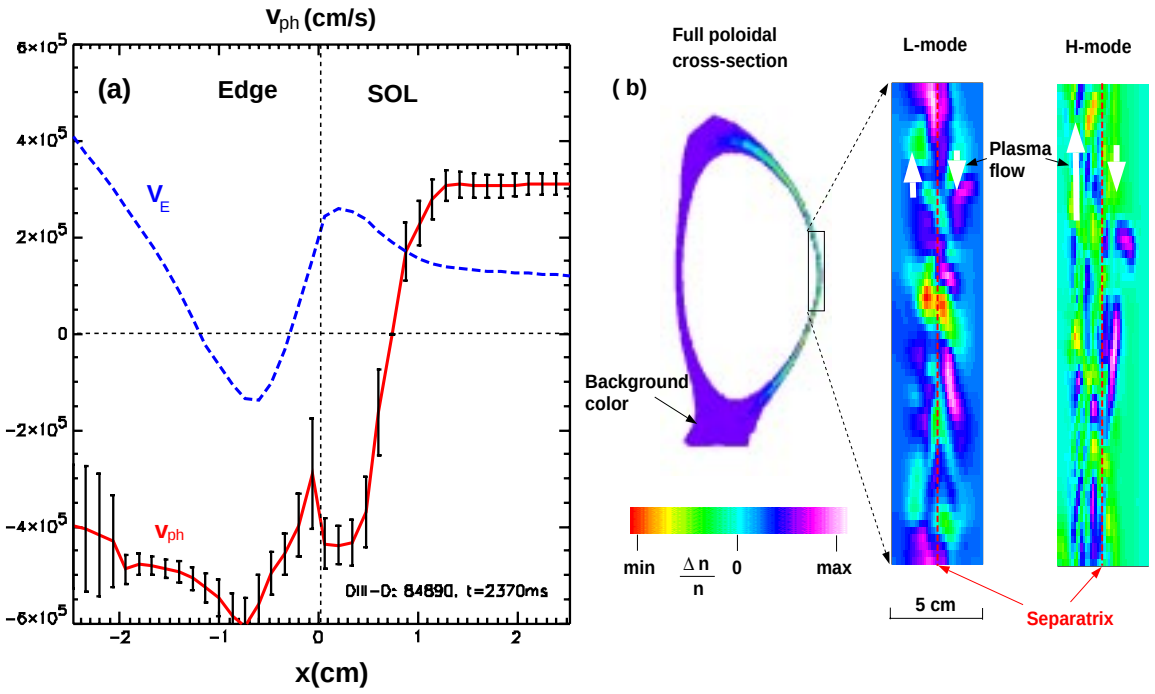

FIG. 2: (a) BOUT fluctuation phase velocity across the magnetic separatrix in boundary region and $\boldsymbol{E} \times \boldsymbol{B}$ velocity; (b) Density fluctuations at outboard midplane, for L-mode $|\Delta n/n| \sim 0.2$ and for H-mode $|\Delta n/n| \sim 0.05$. H-mode structures are broken up by flow shear.

correlation function (in poloidal direction θ and time τ) computed at each radius. Velocity reversal has been observed in tokamaks and stellarators [15]. The figure also indicates that the $\boldsymbol{E} \times \boldsymbol{B}$ velocity differs from the phase velocity. Here the E is the total electric field calculated from BOUT simulations. Theory and interpretations of experimental data based on the common assumption that the phase velocity is controlled by the $\boldsymbol{E} \times \boldsymbol{B}$ velocity have to be modified. Thus in the rest of the paper, we will differentiate the plasma flow $V_P = V_E + V_{\nabla P_i}$ from the poloidal fluctuation phase velocity v_{ph}, where V_E is the $\boldsymbol{E} \times \boldsymbol{B}$ velocity and $V_{\nabla P_i}$ the ion diamagnetic drift velocity. The reversal of the fluctuation phase velocity with x is due to different dynamics inside separatrix and in the SOL. The RX turbulence, mainly inside the separatrix, is driven by electron skin physics coupled with bad curvature. The RX turbulence phase velocity is in the electron drift direction. Due to the X-point physics, the RX turbulence penetrates some way into the SOL. Because of the electron temperature decays faster than the ion temperature in the SOL, the ion diamagnetic drift velocity dominates the phase velocity deeply into the SOL. The energy budget is such that RX turbulence pumps expansion free energy from the plasma pressure gradient into flow energy via mode coupling [16, 8]. The typical fluctuation parameters obtained are a correlation time $\tau_c \sim 15\mu s$ on the midplane, which is in agreement with probe and the PCI measurements [17]. The poloidal correlation length is $\Delta_p \sim 16\rho_s \sim 4$ cm, the radial correlation length $\Delta_r \sim 5\rho_s \sim 1$ cm, and the poloidal propagation velocity v_{ph} ~ -500m/s in the edge and $v_{ph} \sim 300$m/s in SOL. The radial correlation length is smaller than the poloidal correlation length by a factor of 4, indicating oblique structures in the poloidal-radial plane. In the direction parallel to the magnetic field, the correlation length $\Delta_{||}$ is very long, $\Delta_{||} \simeq \pi q R \sim 10$m. The boundary plasma turbulence thus has a filamentary structure extending only a few cm perpendicular to the

magnetic field but many meters in the parallel direction. These filaments are qualitatively consistent with the experimental observations from high speed movies and videos [18]. The poloidal projection of the filaments has been also called 'eddies' as shown in Fig. 2(b). For fixed background plasma profiles, there is almost no radial propagation of the turbulence. In a dynamically steady state with the sources and sinks, a very low radial (as compared to poloidal) propagation velocities of 200m/s outward has been found.

Particle transport perpendicular to the magnetic field Γ_r results from correlated fluctuations of the plasma drift velocity $\tilde{v}_E$ and density $\tilde{n}$, and can be calculated from $\Gamma_r = \langle \tilde{v}_E \tilde{n} \rangle$. A strong poloidal asymmetry of the turbulent flux of particles is shown in Fig. 3(a). Due

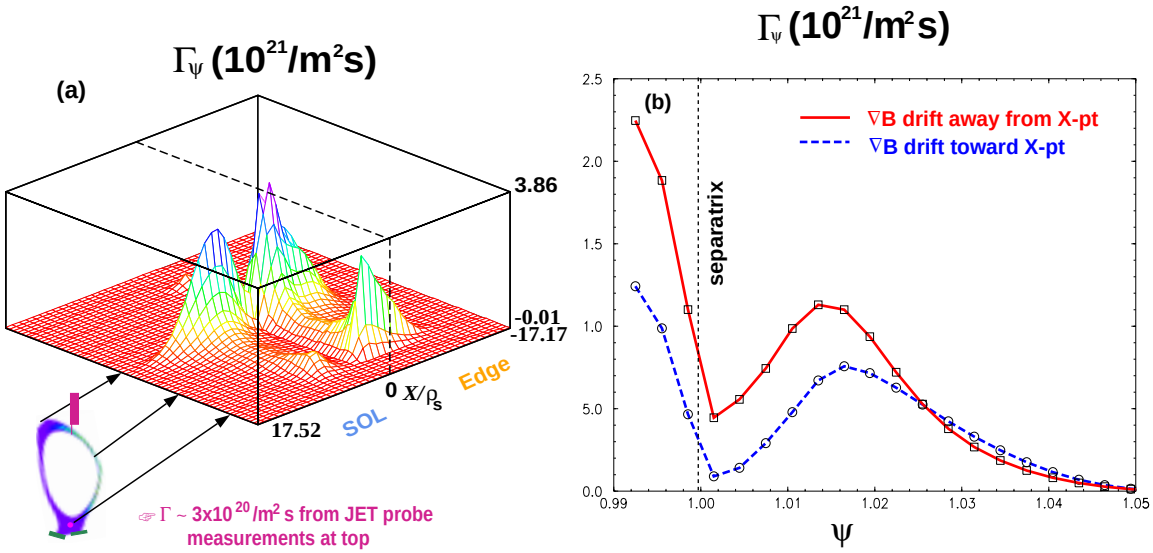

FIG. 3: (3a)The turbulent particle flux in radial-poloidal plane; (3b)The flux surface averaged turbulent particle flux for the ion ∇B drift towards the X-point (solid line) and ion ∇B drift away from the X-point (dashed line).

to the X-point null, the plasma drift velocity $\tilde{v}_E \propto k_p \propto nB_t/RB_p$ diverges there as $B_p \to 0$, and thus a large particle flux is produced near the X-point region. The poloidal asymmetry of the turbulent particle flux has been reported experimentally on the limiter machines with a factor of 2 larger in low field side than high field side [19]. However, there is a much stronger poloidal asymmetry in X-point divertor geometry. This also solves the paradox from the JET probe measurements [20], where it has been reported that *the maximum of the turbulent particle flux is about a factor (3-5) larger than in limiter magnetic configuration, for similar plasma parameters, which seems to be in contradiction with the plasma global particle confinement times.* To understand the paradox, we have to understand the setup of the experiments. The turbulent particle transport has been measured in JET with a Langmuir probe array system installed on the top of the machine on the low-field side as shown in Fig. 3(a). It is then commonly assumed that the turbulent particle flux measured locally at that position is characteristic of the whole surface of the torus. For a limiter machine, an agreement within a factor of two usually was found. However, in divertor machines it can be off as much as a factor of 10 as shown in Fig. 3(a).

2.2 The effect of direction of toroidal field on the RX mode

The ion ∇B drift direction affects the H-mode power threshold (P_{TH}), where factors of 2-3 increase in P_{TH} are observed for the ion ∇B drift away from the X-point. The BOUT simulation results show the sensitivity of the turbulence to the direction of the toroidal magnetic field B_t [8]. It has been shown that the poloidal flow V_P changes sign when the direction of B_t is reversed keeping everything else the same [8]. However, the simulation results show that the phase velocity v_{ph} keeps the same sign, indicating $|v_{ph}| > |V_P|$. The lower fluctuation levels in the case of the ion ∇B drift towards the X-point than the ion ∇B drift away from the X-point in SN divertor tokamaks was observed due to a change in boundary plasma flow direction away from X-point that impacts the strong damping near the divertor X-point [8]. The poloidal averaged particle transport in the case of the ion ∇B drift towards the X-point is about a factor of 2 smaller than the ion ∇B drift away from the X-point as shown in Fig. 3(b). The probe data generally show a qualitatively agreement with Fig. 3(b) to the extent that the flux passes through a minimum just outside the separatrix on the outboard midplane for the case of the ion ∇B drift towards the X-point, where Fig. 3(b) has a minimum radially. However the two ∇B drift cases have comparable fluxes experimentally, indicating that the difference indeed mostly comes from X-point regions.

2.3 Single-null vs. Double-null geometry

Experimental evidence suggests that the L-H transition threshold is often higher in DN divertors than in SN divertors. From power balance, the power threshold is proportional to the anomalous transport. The higher power threshold means higher the fluctuation and transport. To elucidate the role of the magnetic geometry, we use the same plasma profiles for both SN and DN configuration. Figures 4 shows that the RX modes are still the dominant mode in DN and the density fluctuation level is higher than SN by a factor of 2. The reason is that as the top X-point moves close to the separatrix, the strong X-point shear prevents the RX mode to penetrate into the good curvature side. Thus, there is more averaged bad curvature drive seen by RX mode in DN. It is worthwhile to point out that in recent experiments on DIII-D, contrary to previous experience, the balanced DN had lower H-mode power threshold than SN. One possible difference would be higher triangularity and better X-point control. The corresponding simulations are under investigation.

3. L-H transitions with sources and sinks

Since the RX turbulence model seems to reproduce many of the features of the boundary fluctuation and transport, the properties of the L-H transition has also been explored [8]. In that work we find that under DIII-D tokamak L-mode conditions, the dominant source of turbulence is curvature-driven RX modes. With heat sources added in the core-edge region and sinks in the scrape-off layer (SOL), the code follows the self-consistent profile evolution together with turbulence. Results indicate that, as the power is increased, these modes are stabilized by increased turbulence-generated velocity shear, resulting in an abrupt suppression of high-n turbulence and formation of a pedestal in density and temperature, as is characteristic of the H-mode transition. Owing to the three dimensional nature of the problem, a simple scaling dependence of the power threshold has not yet been produced. Nevertheless, it is clearly shown that the L-H transition and the suppression of the turbulence results when sources of energy drive sufficient pressure gradients,

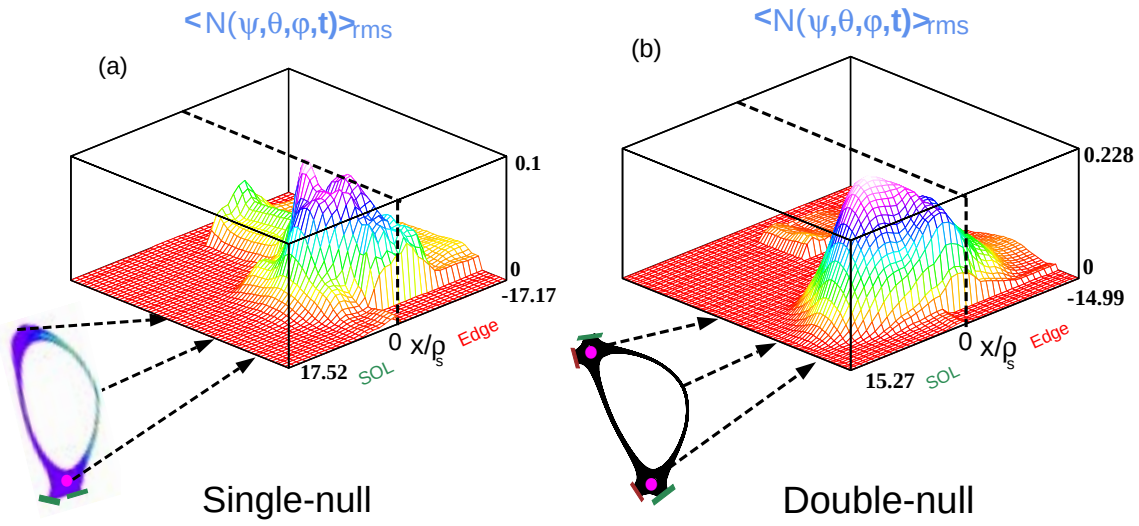

FIG. 4: (a) Ensemble averaged density fluctuation in SN X-point geometry; (b) Ensemble averaged density fluctuation in double-null X-point geometry.

as in the experiments.

We now demonstrate the L-H transition in the BOUT simulation, where the density profile is allowed to evolve. Since the temperature profile remains fixed, the model implies an energy source that heats the new particles to the background level; experimentally this is achieved by adding auxiliary heating to pellet injection [21]. The density source term is of the form

$$S(x) = s_0 \hat{S}(x), \qquad \hat{S}(x) = exp\left(-\frac{(x - X_L)^2}{\Delta_s^2}\right). \tag{1}$$

This source term exhibits a maximum at the left boundary $x = X_L$ and is such that it decreases rapidly when approaching the separatrix with the source amplitude s_0 and the width Δ_s . The reason for this choice is to simulate the power from the core and turbulence transport of the energy across the edge region into the SOL. The link between the source amplitude and the total input power P_{input} is given by

$$P_{input} \simeq \frac{\sqrt{\pi}}{2} s_0 \Omega_{ci} N_i T_i V, \qquad V = 2\pi^2 Ra\Delta_s. \tag{2}$$

where Ω_{ci} is the ion gyrofrequency, V the source volume, N_i the ion density, the ion temperature, R the major radius, and a the minor radius. In this model, the edge gradient adjusts itself such that the time average of the flux out of the volume balances the input flux (the radial integral of the source S). Figure 5(a) shows the density profile for various source amplitude s_0. Clearly, the density and ion pressure profile steepen as the source amplitude increases. The time evolution of the turbulent electron heat flux $q_{e,\psi} = \langle \tilde{v}_E \tilde{T}_e \rangle$ is illustrated in Fig. 5 (b) for several source rates. In all runs shown in Fig. 5 (b), BOUT starts initially from a very small noise level at $t = 0$ and runs to a saturated state at $t = 4000$ via a linear growth phase. Then from the saturated state, the various energetic particle sources are turned on to evolve into a new steady state, corresponding to L-mode and H-mode phase. It is clearly shown that for large input power, the turbulence electron heat flux is suppressed by a factor of 4. For the case of high source amplitude

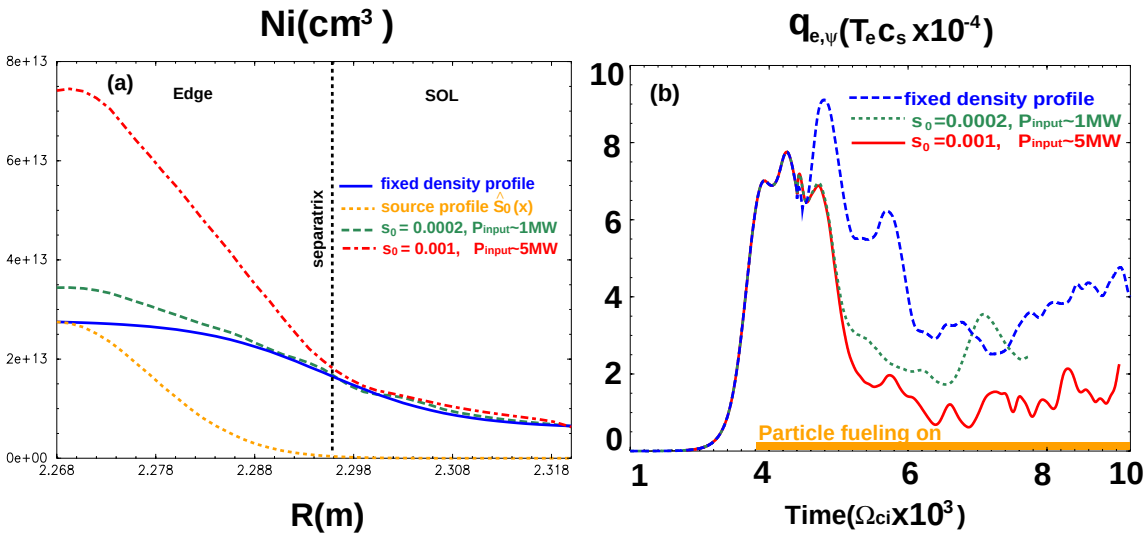

FIG. 5: (a) Plasma density profiles for the various energetic particle fueling; (b) Time history of the electron conduction heat flux.

with L-H transition, the corresponding $\boldsymbol{E} \times \boldsymbol{B}$ velocity and the fluctuation phase velocity is given in Figure 6(a). It is shown that the $\boldsymbol{E} \times \boldsymbol{B}$ velocity increases by a factor of 7 and the phase velocity by a factor of 2 after the transition, as compared to corresponding velocity in Fig. 2(a). However, the phase velocity is still larger than the $\boldsymbol{E} \times \boldsymbol{B}$ velocity by a factor of 2. As discussed in Ref. [8], the flow shear is produced by poloidal spin-up driven by the turbulence-generated radial current near the transition. After the transition the fluctuations are quenched, and therefore the drive for the flow shear vanishes but the ∇P_i contribution remains. Therefore the turbulent suppression remains as well. This feature is in qualitative agreement with phase-transition models [22] and the nonlinear simulations of resistive pressure gradient driven turbulence [23]. The radial profiles of the electron heat flux indicate global suppression, as shown in Figure 6(b). In our previous BOUT simulations [8], we used an ion energy source with fixed density profile to simulate neutral beam heating. In this work, we ramp up the density profile while keeping the ion temperature constant. Although the final plasma pressure profile is similar via either route, we find it is easy to maintain the H-mode by heating ions directly because it is easy to get large negative of E_r shear. For the pellet injection $T_i \sim const.$, $E_r \propto (T_i/Zen)dn/dr \rightarrow -T_i/Ze\Delta_s$ as $n \rightarrow \infty$ and Δ_s is shear layer width. For the neutral beam heating $n \sim const.$, $E_r \sim (1/Ze)dT_i/dr \propto -T_i/\Delta_s$ and $E_r \rightarrow -\infty$ as $T_i \rightarrow \infty$.

4. Summary and conclusions

BOUT contains much of the relevant physics for the pedestal barrier problem for the experimentally relevant X-point divertor geometry. Encouraging results have been obtained when using measured DIII-D profiles. The resistive X-point mode has been identified. Comparison of the shifted-circle vs. X-point geometry show the different dominant modes and turbulence fluctuation levels. The poloidal fluctuation phase velocity shows experimentally observed structure across the separatrix in many fusion devices. The fluctuation phase velocity is larger than $E \times B$ velocity. A strong poloidal asymmetry of particle flux in the proximity of the separatrix may explain the paradox of the JET probe measure-

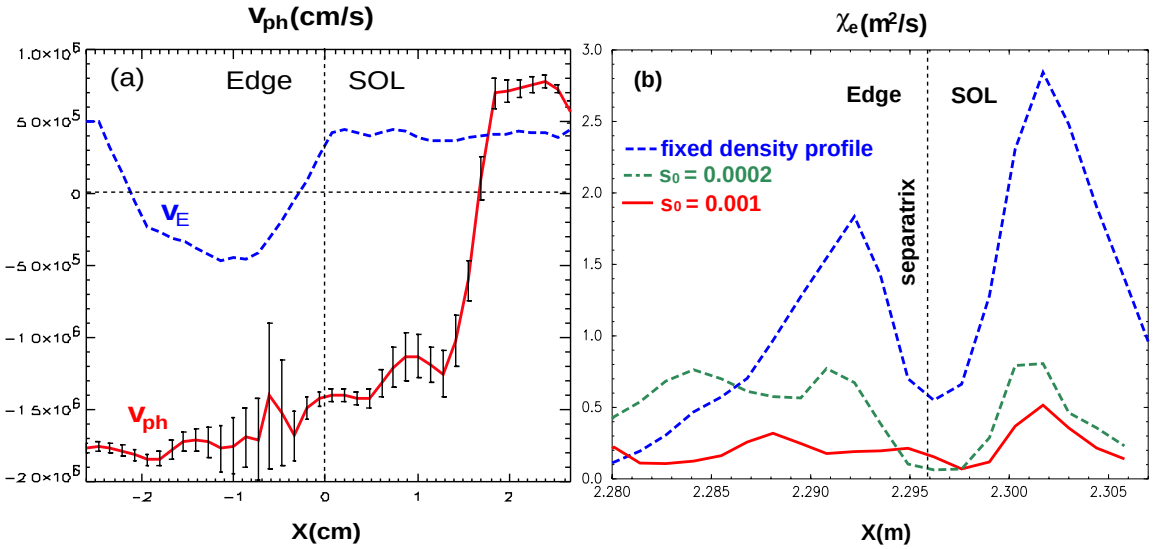

FIG. 6: (a). Radial profiles of $\boldsymbol{E} \times \boldsymbol{B}$ *velocity and fluctuation phase velocity across the separatrix for* $s_0 = 0.001$ *in Fig. 5; (b).Radial profiles of electron heat diffusivity for the corresponding particle fueling.*

ment of the particle flux when comparisons of the limiter vs. divertor experiments had been made. Our L-H transition with simple sources added shows transitions with resistive X-point modes dominating L-mode. The levels of turbulence are similar to experimental measurements. We also show that the poloidal averaged particle transport in the case of the ion ∇B drift towards the X-point is about a factor of 2 smaller than the ion ∇B drift away from the X-point. The difference may mostly comes from the direction of the plasma flow in the X-point regions.

5. ACKNOWLEDGMENTS

The simulations were done on the NERSC T3E and IBM SP, and on Livermore Computing/LLNL workstation clusters. We thank Drs. K. H. Burrell, P. H. Diamond, A. M. Dimits, R. J. Groebner, T. S. Hahm, S. Krasheninnikov, L. L. Lao, T. L. Rhodes, L. L. Lodestro, G. R. Mckee, L. D. Pearlstein, M. N. Rosenbluth, D. D. Ryutov, T. C. Simonen, and S. Zweben for fruitful physics discussions. We thank for Dr. A. Hindmarsh and A. Taylor on providing the PVODE PDE Solver package.

References

[1] Burrell, K. H., Phys. of Plasmas, Vol. **4** (1997) 1499.

[2] Moyer R A, Phys. of Plasmas, Vol. **2** (1995) 2397.

[3] Carlstrom, T. N. Gohil, P., Watkins, J. G, *et al.*, Plasma Phys. Control. Fusion **36** A147(1994).

[4] Horton, L. D., Plasma Phys. Control. Fusion **42**, (2000) A37-A49.

[5] Carlstrom, T. N., Burrell, K. H., Groebner, R. J., *et al.*, *Importance of X-point Physics on the H-mode Power Threshold in DIII-D*, GO2, 41st APS Meeting,1999.

[6] Xu, X. Q., and Cohen, R. H., Contributions to Plasma Physics, Vol. **38** (1998) 158.

[7] Braginskii, S. I., Transport processes in a plasma *Reviews of Plasma Physics*, Vol. I, Ed. M. A. Leontovich (Consultants Bureau, New York, 1965), p. 205.

[8] Xu, X. Q., Cohen, R. H., Rognlien, T. D., and Myra, J. R., Phys. of Plasmas, Vol. **7**, (2000) 1951.

[9] Ryutov, D. D., and Cohen, R. H. *Symmetry Considerations in the Selection of Plasma Transport Models for Tokamaks*, UP2.12, 41st APS Meeting,1999.

[10] Bishop, C. M., Nuclear Fusion, **26**, (1986) 1063.

[11] Hahm, T. S., and Diamond, P. H., Phys. Fluids Vol. **30**, (1987) 137.

[12] Connor,J. N. and Hastie, R. J., Phys. of Plasmas, Vol. **6**, (1999) 4260.

[13] Xu, X. Q., Cohen, R. H., Porter, *et al.*, Nuclear Fusion, Vol. 40, (2000) 731.

[14] Myra, J. R., D'Ippolito, D. A., Xu, X. Q., and Cohen, R. H., Phys. of Plasmas, Vol. **7**, (2000) 2290.

[15] Zweben, S. J., *et. al.*, Nuclear Fusion **25** (1985) 171-183; Ritz, Ch. P., *et al.*, Phys. Rev. Lett. **65** (1990) 2543; Hidalgo, C., *et al.*, Nuclear Fusion, **31**, (1991) 1471; Antoni, V., *et al.*, Phys. Rev. Lett. **79** (1997) 4814.

[16] Diamond, P. H., *et. al.*, Phys. Rev. Lett. **84** 4842 (2000) 4842; Diamond, P. H., Rosenbluth, M. N., *et. al.*, in Plasma Physics and Controlled Nuclear Fusion Research, 1998, (Proc. 17th Int. Conf. Yokohama, 1998), Vol. **IV**, IAEA Vienna (1999) 1421; Sanchez, E., *et. al.* , Phys. of Plasmas, **7** (2000) 1408;

[17] C. Rost, *et al.*, in Controlled Fusion and Plasma Physics (Proc. 27th EPS Conf. Budapest, Europhysics Conference Abstracts, Geneva, 2000).

[18] S. Zweben, *et al.*, in Controlled Fusion and Plasma Physics (Proc. 27th EPS Conf. Budapest, Europhysics Conference Abstracts, Geneva, 2000); Endler, M., J. Nucl. Mater. **266-269** (1999)84-90.

[19] Tynan, G. R., 1996 Transport, Chaos and Plasma Physics 2. Equ. Turbulence Plasma (Universite de Provence, IMT Marseille, 10-22 July, 1995) (Singapore: World Scientific)

[20] Garcia-Cortes, I., *et al.*, in Plasma-surface interactions in Controlled Fusion Devices, (Proc. 14th PSI Conf. Rosenheim); Garcia-Cortes, I., *et al.*,Plasma Phys Control. Fusion, **42** (2000) 389-400.

[21] Gohil, P., *et al.*, 2000 US-EU Transport Task Force Workshop (Burlington, USA), unpublished.

[22] Diamond, P. H., Liang, Y-M, Carreras, B. A. and Terry, P. W., 1994 Phys. Rev. Lett. **72** 2565.

[23] Carreras, B. A., Lynch, V. E., Garcia, L., and Diamond, P. H., Phys. of Plasmas, Vol. **2**, 2722 (1995).